

Stability Analysis for Cosmic-Ray Heating of Cool Cores in Galaxy Clusters

Yutaka Fujita^{1*}, Sota Kimura¹, and Yutaka Ohira²

¹*Department of Earth and Space Science, Graduate School of Science, Osaka University, 1-1 Machikaneyama-cho, Toyonaka, Osaka 560-0043, Japan*

²*Department of Physics and Mathematics, Aoyama Gakuin University, Fuchinobe, Chuou-ku, Sagami-hara 252-5258, Japan*

Accepted 0000 December 15. Received 0000 December 14; in original form 0000 October 11

ABSTRACT

We study the heating of the cool cores in galaxy clusters by cosmic-rays (CRs) accelerated by the central active galactic nuclei (AGNs). We especially focus on the stability of the heating. The CRs stream with Alfvén waves in the intracluster medium (ICM) and heat the ICM. First, assuming that the heating and radiative cooling is balanced, we search steady state solutions for the ICM and CR profiles of clusters by solving a boundary value problem. The boundary conditions are set so that the solutions are consistent with observations of clusters. We find steady state solutions if the magnetic fields are strong enough and the association between the magnetic fields and the ICM is relatively weak. Then, we analyse the stability of the solutions via a Lagrangian perturbation analysis and find that the solutions are globally stable. We confirm the results by numerical simulations. Using the steady state solutions as the initial conditions, we follow the evolution of the profiles for 100 Gyr. We find that the profiles do not evolve on time scales much larger than cluster lifetimes. These results, as well as consistency with observations of radio mini-halos, suggest that the CR heating is a promising mechanism to solve the so-called “cooling flow problem”.

Key words: cosmic rays — cooling flows — galaxies: clusters: general — galaxies: clusters: individual: A1795, A2052, A2199, A2597

1 INTRODUCTION

The radiative cooling time of the intracluster medium (ICM) in the cores of galaxy clusters is often smaller than the age of the clusters (Sarazin 1986). If there were no heating sources, massive cooling flows toward the cluster centres would develop in the cores (Fabian 1994). However, X-ray observations have revealed that such flows do not exist in the cores (e.g. Ikebe et al. 1997; Makishima et al. 2001; Peterson et al. 2001; Tamura et al. 2001; Kaastra et al. 2001; Matsushita et al. 2002). This means that some unknown heating sources prevent such flows from developing (cooling flow problem).

AGNs at the cluster centres are often thought to be the heating sources. However, the energy transfer mechanism from the AGNs to the surrounding ICM is not understood. Conventional mechanical heating (e.g. shocks, or sound waves) may cause thermal instability (Fujita & Suzuki 2005; Mathews, Faltenbacher, & Brighenti 2006). Thus, strong turbulence would be required to stabilise the heating, if the cores are mainly mechanically heated.

Cosmic-rays (CRs) accelerated by the AGNs are another promising carrier of the energy to the ICM (e.g. Tucker & Rosner 1983; Rephaeli 1987; Rephaeli & Silk 1995; Colafrancesco, Dar, & De Rújula 2004; Pfrommer et al. 2007; Jubelgas et al. 2008). CR streaming is one way to deposit their energy into the ICM (Rephaeli 1979; Boehringer & Morfill 1988; Loewenstein, Zweibel, & Begelman 1991; Guo & Oh 2008; Pfrommer 2013). Each CR particle moves with a velocity close to the light velocity c . However, in a cluster, they are scattered by Alfvén waves in the ICM. Thus, the CRs effectively move along with the waves with a bulk (streaming) velocity v_{st} , which is much smaller than c . Since the CR pressure is high around the central AGN and waves are excited in the direction of the CR pressure gradient (e.g. Longair 1994), the waves and the CRs scattered by them move outward in the cluster in general. As a result, the CR pressure does PdV work against the ICM, which ultimately heats the ICM. Using numerical simulations, we showed that the ICM can be stably heated by the CR streaming (Fujita & Ohira 2011, hereafter Paper I). The main reason of the stability is that the CRs stream in the ICM and the heating is not localised around the AGN. In successive

* E-mail: fujita@vega.ess.sci.osaka-u.ac.jp

studies, we calculated non-thermal emissions from the CRs (Fujita & Ohira 2012, hereafter Paper II), and we showed that the radial profiles of radio mini-halos observed in clusters can be reproduced in our model (Fujita & Ohira 2013, hereafter Paper III).

In this paper, we study the reason of the stability of the CR heating in more detail based on a perturbation analysis and numerical simulations. This paper is organised as follows. In § 2, we explain our models and show the basic equations. In § 3, we solve those equations and obtain steady state solutions when the CR streaming velocity is the Alfvén velocity. Moreover, we analyse the stability of the steady state solutions. In § 4, we discuss the evolution of the ICM with time and radio mini-halos observed around cluster cores. § 5 is devoted to conclusions. Throughout this paper we assume a Λ CDM cosmology with $\Omega_m = 0.3$, $\Omega_\Lambda = 0.7$, and $h = 0.7$, where $H_0 = 100 h \text{ km s}^{-1} \text{ Mpc}^{-1}$. We consider protons as CRs unless otherwise mentioned.

2 MODELS

2.1 Equations

The model we adopt in this study is basically the same as that in Papers I–III. Assuming that the cluster is spherically symmetric, the flow equations are

$$\frac{\partial \rho}{\partial t} + \frac{1}{r^2} \frac{\partial}{\partial r} (r^2 \rho u) = 0, \quad (1)$$

$$\frac{\partial (\rho u)}{\partial t} + \frac{1}{r^2} \frac{\partial}{\partial r} (r^2 \rho u^2) = \rho g - \frac{\partial}{\partial r} (P_g + P_c + P_B), \quad (2)$$

$$\begin{aligned} \frac{\partial e_g}{\partial t} + \frac{1}{r^2} \frac{\partial}{\partial r} (r^2 u e_g) &= -P_g \frac{1}{r^2} \frac{\partial}{\partial r} (r^2 u) \\ &+ \frac{1}{r^2} \frac{\partial}{\partial r} \left[r^2 \kappa(T) \frac{\partial T}{\partial r} \right] - n_e^2 \Lambda(T) + H_{\text{st}} + H_{\text{coll}}, \end{aligned} \quad (3)$$

$$\begin{aligned} \frac{\partial e_c}{\partial t} + \frac{1}{r^2} \frac{\partial}{\partial r} (r^2 \tilde{u} e_c) &= -P_c \frac{1}{r^2} \frac{\partial}{\partial r} (r^2 \tilde{u}) \\ &+ \frac{1}{r^2} \frac{\partial}{\partial r} \left[r^2 D(\rho) \frac{\partial e_c}{\partial r} \right] - \Gamma_{\text{loss}} + \dot{S}_c, \end{aligned} \quad (4)$$

where ρ is the gas density, u is the gas velocity, P_g is the gas pressure, P_c is the CR pressure, P_B is the magnetic pressure, g is the gravitational acceleration, $\kappa(T)$ is the coefficient for thermal conduction, T is the temperature, n_e is the electron density, Λ is the cooling function, H_{st} is the heating by CR streaming, H_{coll} is the heating by Coulomb and hadronic collisions, \tilde{u} is the CR transport velocity, $D(\rho)$ is the diffusion coefficient for CRs averaged over the CR spectrum, Γ_{loss} is the energy loss by Coulomb and hadronic collisions, and \dot{S}_c is the source term of CRs. Energy densities of the gas and the CRs are respectively defined as $e_g = P_g/(\gamma_g - 1)$ and $e_c = P_c/(\gamma_c - 1)$, where $\gamma_g (= 5/3)$ and γ_c are the adiabatic indices for the ICM and CRs, respectively. For the latter, we assume $\gamma_c = 5/3$, because we found that the energy spectrum of the CRs must be steep and most of the CRs have low energies by comparing model predictions with radio observations (Papers II and III).

Since we later perform a perturbation analysis, we need to make the model simpler. We do not include thermal conduction and CR diffusion ($\kappa = 0$ and $D = 0$). For the same

reason, we assume a simple cooling function:

$$\begin{aligned} n_e^2 \Lambda(T) &= \rho \mathcal{L} \\ &= 2.1 \times 10^{-27} \left(\frac{n_e}{\text{cm}^{-3}} \right)^2 \left(\frac{T}{\text{K}} \right)^{1/2} \text{ erg cm}^{-3} \text{ s}^{-1} \end{aligned} \quad (5)$$

(Rybicki & Lightman 1979; Kim & Narayan 2003; Guo, Oh, & Ruszkowski 2008). We also ignore the gradient of magnetic pressure ($\partial P_B / \partial r = 0$) in equation (2), because it is not dynamically important.

2.2 AGN

In our model, CRs are accelerated by the central AGN. The source term of the CRs is given by

$$\begin{aligned} \dot{S}_c &= \frac{3 - \nu}{4\pi} \frac{L_{\text{AGN}}}{r_1^3 (r_1/r_0)^{-\nu} - r_0^3} \left(\frac{r}{r_0} \right)^{-\nu} \\ &\times (1 - e^{-(r/r_0)^2}) e^{-(r/r_1)^2}, \end{aligned} \quad (6)$$

where L_{AGN} is the energy injection rate from the AGN. We assume that

$$\begin{aligned} L_{\text{AGN}} &= -\epsilon \dot{M} c^2 \\ &= 1.4 \times 10^{44} \text{ erg s}^{-1} \left(\frac{\epsilon}{2.5 \times 10^{-4}} \right) \left(\frac{-\dot{M}}{10 M_\odot \text{ yr}^{-1}} \right), \end{aligned} \quad (7)$$

where ϵ is the parameter, and \dot{M} is the flow rate of the gas. In this model, accelerated CRs are first carried by buoyant bubbles from the AGN out to large distances (Guo & Oh 2008). As the bubbles filled with the CRs adiabatically rise, the CRs may escape from the bubbles into the ICM or they may be injected into the ICM through the shredding of the bubbles by Rayleigh-Taylor and Kelvin-Helmholtz instabilities. Thus, the CRs are gradually injected into the ICM as the buoyant bubbles rise. Unless otherwise mentioned, we fixed the parameters at the values similar to the ones used in Papers I–III ($\epsilon = 2.5 \times 10^{-4}$, $\nu = 3.2$, $r_0 = 20 \text{ kpc}$, and $r_1 = 150 \text{ kpc}$), because they give results that are consistent with observations (see later). In Papers I and II, we assumed that the CRs are accelerated at the forward shock of a cocoon created through the AGN activities. However, it may be more appropriate to assume that CR protons are accelerated around the central black hole and that AGN jets or winds consist of the CR protons, especially when ϵ is large (§ 3.1 of Paper III; see also Sikora et al. 2005; Toma & Takahara 2012).

2.3 Cosmic-rays

The CR transport velocity is given by $\tilde{u} = u + v_{\text{st}}$ in equation (4). The most simple idea is that v_{st} is the Alfvén velocity v_A , because the CRs are scattered by the Alfvén waves and move with them. However, there have been debates about this issue. It has been indicated that v_{st} may be much larger than v_A , because in hot ICM, Alfvén waves may damp at small wave lengths via interactions with thermal protons. In this case, the sound velocity of the gas c_s may be more plausible as the streaming velocity (Holman, Ionson, & Scott 1979; Enßlin et al. 2011). However, there also have been indications that the deficit of the scattering at short wave lengths is overcome by other effects such as mirror scattering or wave

cascading (e.g. Felice & Kulsrud 2001; Schlickeiser 2002; Wiener, Oh, & Guo 2013). If this is the case, the assumption of $v_{\text{st}} = v_A$ is appropriate. We consider the latter case ($v_{\text{st}} = v_A$) in the following sections. We discuss the former case ($v_{\text{st}} = c_s$) in Appendix.

In this study, we investigate steady state solutions. Therefore, we assume that the growth of the waves is balanced with non-linear wave damping. In other words, the CR energy consumed to grow the waves is equal to the wave energy that is put into the ICM through the wave damping. Thus, the heating term of the CR streaming is given by

$$H_{\text{st}} = -v_{\text{st}} \frac{\partial P_c}{\partial r}. \quad (8)$$

Note that $v_{\text{st}} > 0$ and $\partial P_c / \partial r < 0$ in our calculations.

In Papers I and II, we studied the evolution of wave amplification. In those studies, we conservatively assumed that the balance between the wave growth and the damping is archived when the wave energy density reaches to that of the background magnetic fields, because some of non-linear damping mechanisms should be effective after that. As shown in Paper I (its Fig. 3), the time scale in which the growth and the damping is balanced is \sim Gyr. Since it is less than the time scale of a cluster lifetime (~ 10 Gyr), the assumption of the balance in this study is justified. Moreover, if the damping is very efficient, the saturation may be achieved even faster. For example, if the time scale of the damping is proportional to the inverse of the gyro frequency of CR particles (e.g. non-linear Landau damping; Felice & Kulsrud 2001), the saturated wave energy density is much smaller than that of the background magnetic fields.

We ignore Coulomb and hadronic collisions ($H_{\text{coll}}=0$ and $\Gamma_{\text{loss}}=0$) in equations (3) and (4), because they do not much affect the results as follows (see also Papers I and III). The collisional heating term is given by $H_{\text{coll}} = -\Gamma_c - \Gamma_h/6$, and the loss term is given by $\Gamma_{\text{loss}} = -\Gamma_c - \Gamma_h$, where Γ_c is the Coulomb loss rate and Γ_h is the hadronic loss rate (Paper III). In Paper III, we estimated that

$$\Gamma_c = \chi_c \left(\frac{n_e}{\text{cm}^{-3}} \right) \left(\frac{e_c}{\text{erg cm}^{-3}} \right) \text{erg s}^{-1} \text{cm}^{-3}, \quad (9)$$

$$\Gamma_h = \chi_h \left(\frac{n_e}{\text{cm}^{-3}} \right) \left(\frac{e_c}{\text{erg cm}^{-3}} \right) \text{erg s}^{-1} \text{cm}^{-3}, \quad (10)$$

where $\chi_c = -7.3 \times 10^{-16}$ and $\chi_h = -1.5 \times 10^{-17}$. In these estimations, we assumed that the CR momentum spectrum is given by a power law ($\propto p^x$), and the index is $x = 3$. We chose $x = 3$ because it is consistent with observations of radio mini-halos in clusters (Paper III). Moreover, we assumed that the minimum momentum is $p_{\text{min}}c = 137$ MeV, at which the effect of Coulomb collision is maximum (Paper III). For these values, we have confirmed that H_{coll} and Γ_{loss} can be ignored for the results in the following sections. We note that the index could be as large as $x = 3.5$ to be consistent with the observations when $v_{\text{st}} = v_A$ (Paper III). We estimated $\Gamma_c/(n_e e_c)$ and $\Gamma_h/(n_e e_c)$ for $x = 3.5$ and $p_{\text{min}}c = 137$ MeV, and found that $\chi_c = -7.6 \times 10^{-16}$ and $\chi_h = -4.9 \times 10^{-18}$. Thus, $H_{\text{coll}}/(n_e e_c)$ and $\Gamma_{\text{loss}}/(n_e e_c)$ are not much different from those when $x = 3$ and $p_{\text{min}}c = 137$ MeV.

We also changed $p_{\text{min}}c$ for $x = 3$. When $p_{\text{min}}c = 43$ MeV, $\chi_c = -2.7 \times 10^{-16}$ and $\chi_h = -1.6 \times 10^{-18}$, and when $p_{\text{min}}c = 440$ MeV, $\chi_c = -3.8 \times 10^{-16}$ and $\chi_h = -1.2 \times 10^{-16}$. These

mean that $H_{\text{coll}}/(n_e e_c)$ and $\Gamma_{\text{loss}}/(n_e e_c)$ are smaller than those when $p_{\text{min}}c = 137$ MeV. Thus, we can ignore H_{coll} and Γ_{loss} . It is to be noted that when $x > 3$, one can obtain $\Gamma_c/(n_e e_c) \propto p_{\text{min}}^2$ regardless of x in the limit of small p_{min} (see equations [7] and [8] in Paper III).

2.4 Cluster

For the gravitational mass profile, we adopt the NFW model (Navarro, Frenk, & White 1997), although there is a debate about the slope of the central cusp (e.g. Fukushige & Makino 1997). For the NFW profile, the mass distribution is written as

$$M(r) = M_{200} \frac{\ln(1+r/r_s) - r/r_s/(1+r/r_s)}{\ln(1+c_{200}) - c_{200}/(1+c_{200})}. \quad (11)$$

For this equation, we define r_q as the cluster radius within which the average mass density is q times the critical density of the universe $\rho_{\text{cr}}(z)$ at redshift z . Moreover, M_q is the mass of the cluster within r_q , r_s is the characteristic radius, and $c_q = r_q/r_s$. In equation (11), we set $q = 200$. From the definition, we have

$$r_q = \left[\frac{3M_q}{4\pi q \rho_{\text{cr}}(z)} \right]^{1/3}. \quad (12)$$

The mass M_{200} is derived from the ICM temperature outside the core, T_{out} . Based on a statistical study, Chen et al. (2007) obtained a scaling relation of

$$M_{500} = 2.6 \times 10^{14} h^{-1} \left(\frac{T_{\text{out}}}{4 \text{ keV}} \right)^{1.48} M_{\odot}. \quad (13)$$

If we assume the NFW profile, M_{500} can be converted to M_{200} using a relation of $M_q \propto q^{-0.266}$ (Horner, Mushotzky, & Scharf 1999). Theoretically, c_{200} is expected to be a weakly decreasing function of M_{200} (e.g. Duffy et al. 2008). However, observations have shown that it has a very large scatter (Okabe et al. 2010; Etori et al. 2010), which may reflect a broad range of the formation epochs of clusters with a give mass (e.g. Fujita & Takahara 1999). Thus, we fix it at $c_{200} = 5$. Using equations (11)–(13), we can determine $M(r)$ of a cluster with given T_{out} and z . The gravitational acceleration for the NFW profile is $g_{\text{NFW}}(r) = -GM(r)/r^2$.

In addition to g_{NFW} , we include the gravitation from the central cD galaxy. We use the one obtained by Mathews, Faltenbacher, & Brighenti (2006) and used in Papers I-III:

$$g_{\text{cD}}(r) = \left[\left(\frac{r^{0.5975}}{3.206 \times 10^{-7}} \right)^s + \left(\frac{r^{1.849}}{1.861 \times 10^{-6}} \right)^s \right]^{-1/s} \quad (14)$$

in cgs with $s = 0.9$ and r in kpc. We assume that g_{cD} does not depend on host clusters. Thus, the total gravitational acceleration in a cluster is $g = g_{\text{NFW}} + g_{\text{cD}}$. The inclusion of g_{cD} does not qualitatively change the results.

3 RESULTS

3.1 Steady State Solutions

First, we derive steady state solutions ($\partial/\partial t = 0$). The procedure is basically the same as that in previous studies (Kim & Narayan 2003; Guo, Oh, & Ruszkowski 2008).

From equation (1), the mass flow rate is given by $\dot{M} = 4\pi r^2 \rho u$. Other three equations (2)–(4) can be rewritten as

$$\frac{1}{r^2} \frac{d}{dr} (r^2 \rho u^2) = -\rho \frac{GM(r)}{r^2} - \frac{d}{dr} (P_g + P_c), \quad (15)$$

$$\frac{1}{r^2} \frac{d}{dr} (r^2 u e_g) = -P_g \frac{1}{r^2} \frac{d}{dr} (r^2 u) - n_e^2 \Lambda(T) + H_{st}, \quad (16)$$

$$\frac{1}{r^2} \frac{d}{dr} (r^2 \tilde{u} e_c) = -P_c \frac{1}{r^2} \frac{d}{dr} (r^2 \tilde{u}) + \dot{S}_c. \quad (17)$$

We solve these ordinary differential equations for $r_{in} < r < r_{out}$, where $r_{in} = 3$ kpc and $r_{out} = 1$ Mpc using *Mathematica 9*¹. They can be solved as a boundary value problem. We impose the following boundary conditions:

$$n_e(r_{in}) = n_0, \quad (18)$$

$$T(r_{in}) = T_{in}, \quad (19)$$

$$T(r_{out}) = T_{out}, \quad (20)$$

$$P_c(r_{in}) = P_{c0}. \quad (21)$$

Equations (15)–(17) form an eigenvalue problem in which \dot{M} is the eigenvalue.

When $v_{st} = v_A = B/\sqrt{4\pi\rho}$, we need to specify magnetic fields B in the ICM. We assume that $B = B_0 (n_e/0.016 \text{ cm}^{-3})^b$. We could not often find steady state solutions for too small B_0 and/or too large b . Thus, we assume that $B_0 = 1.0 \times 10^{-5} \mu\text{G}$ and $b = 0.4$, although we assumed that $B_0 = 1.0 \times 10^{-5} \mu\text{G}$ and $b = 2/3$ in Paper III. The fairly small value of b may mean that the coupling between magnetic fields and the ICM is weak, which may be realised when the magnetic fields are rather radially extended in a cluster. The small b is also favourable to suppress the development of local instabilities (see § 3.2.2).

We construct steady state solutions for four clusters with various temperatures (A1795, A2199, A2052, and A2597), which were studied by Guo, Oh, & Ruszkowski (2008). In Table 1, we give the boundary values n_0 , T_{in} , and T_{out} when $v_{st} = v_A$, which were chosen to be almost consistent with observations (Figs. 1–4). Although there are no direct observations of P_{c0} , the values of P_{c0}/P_{g0} , where $P_{g0} = P_g(r_{in})$, are chosen so that dP_{c0}/dr is not positive and close to zero at $r = r_{in}$.

Dashed lines in Figs. 1–4 show the steady state solutions we obtained. Derived mass flow rates, \dot{M} , are shown in Table 1. It is to be noted that \dot{M} is the mass flow that passes the inner boundary ($r_{in} = 3$ kpc), and that not all the mass needs to fall into the central black hole. Most of the gas may become cold gas or be consumed by star formation in the central galaxy (e.g. Bregman et al. 2006; McNamara & Nulsen 2012). For comparison, we show observations of the four clusters in the figures. The steady state solutions can generally reproduce the observations. Since our model is rather simple (we do not include additional mechanical heating, for example), we think that it would be useless to perfectly fit the solutions with the observations.

Fig. 5 shows the profiles of P_c , P_B , u , H_{st} , and \dot{S}_c for the steady state solution of A1795. The results are qualitatively the same for the other clusters. The pressures (P_c and P_B) and the infall velocity ($-u$) increase toward the cluster

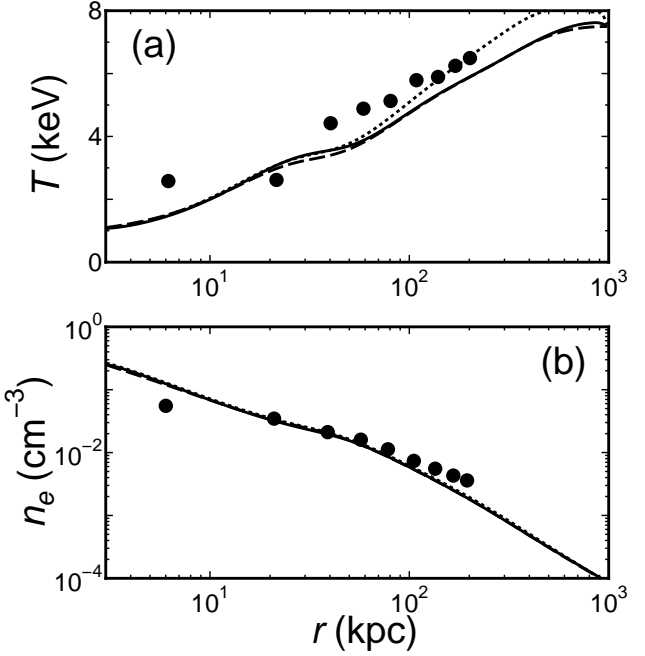


Figure 1. (a) Temperature and (b) density profiles for A1795. Dashed lines show the steady state solution or the initial profiles for the numerical simulation. Solid and Dotted lines are the results of numerical simulation at $t = 40$ Gyr and 100 Gyr, respectively. Filled circles represent observations (Ettori et al. 2002). Error bars are omitted.

centre (Fig. 5a). Both P_c and P_B are smaller than P_g in the whole region. Although $P_B > P_c$ for $r \gtrsim 200$ kpc, P_B is dynamically unimportant there. Fig. 5b shows that the slope of H_{st} is more gentle than that of \dot{S}_c at $r \gtrsim 4$ kpc. This reflects that some of the CRs injected in the inner core region stream in the ICM and heat the ICM in the outer core region.

3.2 Stability Analysis

3.2.1 Lagrangian Perturbation Analysis

We investigate the stability of the steady state solutions obtained in § 3.1. In this subsection, we study the stability by a Lagrangian perturbation analysis. We focus on the global thermal instability in the ICM. The analysing method is based on that in Kim & Narayan (2003) and Guo, Oh, & Ruszkowski (2008).

The relation between a Lagrangian perturbation operator Δ and an Eulerian perturbation δ is

$$\Delta = \delta + \boldsymbol{\xi} \cdot \nabla, \quad (22)$$

where $\boldsymbol{\xi}$ is the Lagrangian displacement of a fluid element (see Shapiro & Teukolsky 1983, p. 127–147). We consider only radial perturbations and we define the radial component of $\boldsymbol{\xi}$ as $\xi = \Delta r$. In this case, the Lagrangian perturbation has commutation relations of

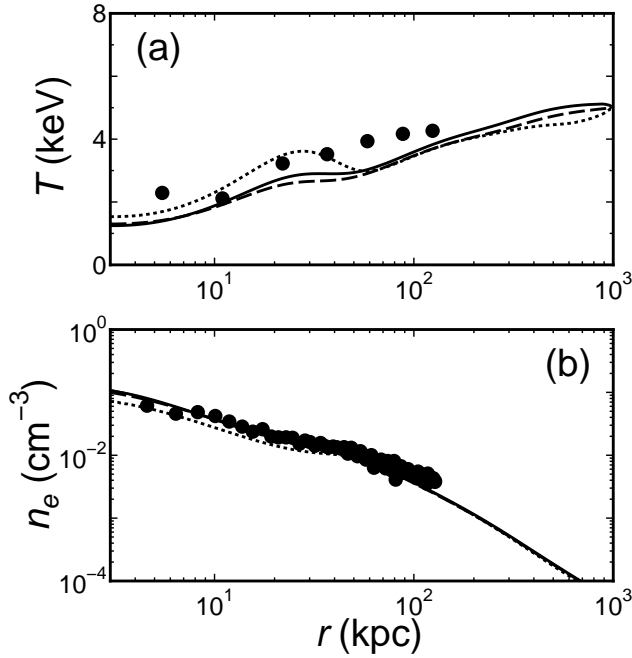
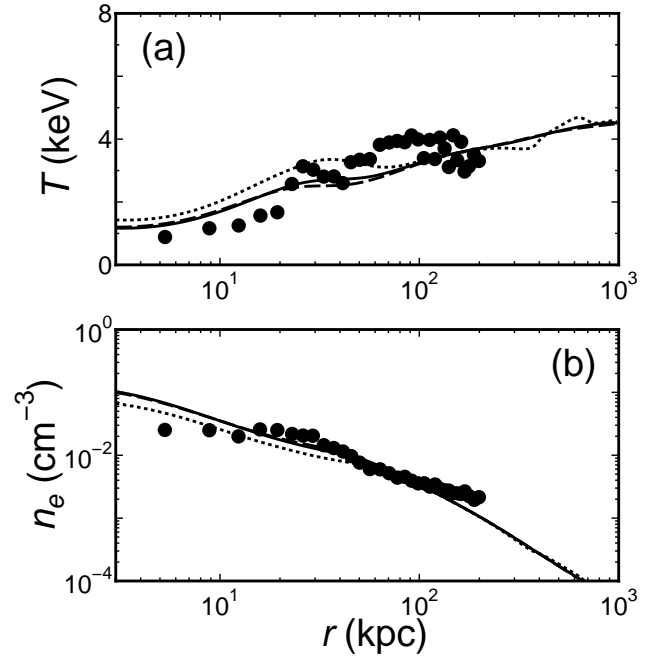
$$\Delta \frac{d}{dt} = \frac{d}{dt} \Delta, \quad (23)$$

$$\Delta \frac{\partial}{\partial r} = \frac{\partial}{\partial r} \Delta - \frac{\partial \xi}{\partial r} \frac{\partial}{\partial r} \quad (24)$$

¹ <http://www.wolfram.com/>

Table 1. Cluster Parameters.

Cluster	z	v_{st}	T_{in} (keV)	T_{out} (keV)	n_0 (cm^{-3})	P_{c0}/P_{g0}	\dot{M} ($M_{\odot}\text{yr}^{-1}$)
A1795	0.0632	v_A	1.1	7.5	0.25	0.15	-27.1
		c_s	1.5	7.5	0.17	0.03	-19.7
A2199	0.0309	v_A	1.3	5	0.1	0.10	-9.2
		c_s	1.5	5	0.1	0.03	-10.4
A2052	0.03549	v_A	1.2	4.5	0.1	0.10	-8.0
		c_s	1.3	4.5	0.1	0.03	-7.4
A2597	0.083	v_A	1.3	4.5	0.1	0.20	-10.4
		c_s	1.4	4.5	0.1	0.03	-9.5


Figure 2. Same as Fig. 1 but for A2199. Filled circles represent observations (Johnstone et al. 2002).

Figure 3. Same as Fig. 1 but for A2052. Filled circles represent observations (Blanton et al. 2011).

(Shapiro & Teukolsky 1983).

Equations (2)–(4) with $\kappa = D = H_{\text{coll}} = \Gamma_{\text{loss}} = \partial P_B / \partial r = 0$ can be rewritten as

$$\rho \frac{du}{dt} = -\frac{\partial P_g}{\partial r} + \rho g, \quad (25)$$

$$\frac{1}{\gamma_g - 1} \frac{dP_g}{dt} - \frac{\gamma_g}{\gamma_g - 1} \frac{P_g}{\rho} \frac{d\rho}{dt} = H_{st} - \rho \mathcal{L}, \quad (26)$$

$$\frac{1}{\gamma_c - 1} \frac{dP_c}{dt} - \frac{\gamma_c}{\gamma_c - 1} \frac{P_c}{\rho} \frac{d\rho}{dt} + \frac{\gamma_c}{\gamma_c - 1} P_c (\nabla \cdot \mathbf{v}_{st}) = \dot{S}_c, \quad (27)$$

where d/dt is the Lagrangian time derivative, and \mathbf{v}_{st} is the streaming velocity including the direction. Equation (1) gives the mass flow rate, $\dot{M} = 4\pi r^2 \rho u$.

We linearize equations (25)–(27). From these equations, and useful relations with gas density and pressure

$$\Delta \rho = -\rho \nabla \cdot \boldsymbol{\xi}, \quad (28)$$

$$\Delta P_g = P_g \frac{\Delta T}{T} - P_g \nabla \cdot \boldsymbol{\xi} \quad (29)$$

(Shapiro & Teukolsky 1983; Guo, Oh, & Ruszkowski 2008),

we obtain following equations:

$$\begin{aligned} \frac{d^2 \xi}{dt^2} &= \frac{P_g}{\rho} \frac{\partial}{\partial r} (\nabla \cdot \boldsymbol{\xi}) \\ &\quad - \frac{1}{\rho} \frac{\partial}{\partial r} \left(P \frac{\Delta T}{T} \right) + \frac{1}{\rho} \frac{\partial P_g}{\partial r} \frac{\partial \xi}{\partial r} - \xi \frac{d^2 \xi}{dr^2}, \end{aligned} \quad (30)$$

$$\begin{aligned} \left(\frac{P_g}{\gamma_g - 1} \frac{d}{dt} + \rho T \mathcal{L}_T + \frac{1}{\gamma_g - 1} \frac{dP_g}{dt} - \frac{\gamma_g}{\gamma_g - 1} \frac{P_g}{\rho} \frac{d\rho}{dt} \right) \frac{\Delta T}{T} \\ + \left(P \frac{d}{dt} - \rho^2 \mathcal{L}_\rho - H_{st} \right) (\nabla \cdot \boldsymbol{\xi}) - \Delta H_{st} = 0, \end{aligned} \quad (31)$$

$$\frac{d}{dt} \left(\frac{\Delta P_c}{P_c} + \gamma_c \nabla \cdot \boldsymbol{\xi} \right) + \gamma_c (\nabla \cdot \mathbf{v}_{st}) = \frac{\Delta \dot{S}_c}{P_c} - \frac{\dot{S}_c \Delta P_c}{P_c^2}, \quad (32)$$

where $\mathcal{L}_T = \partial \mathcal{L} / \partial T|_\rho$ and $\mathcal{L}_\rho = \partial \mathcal{L} / \partial \rho|_T$.

Since $v_{st} = v_A = B / \sqrt{4\pi \rho} \propto \rho^\alpha$, where $\alpha = b - 0.5$, perturbations of v_{st} can be represented by

$$\Delta v_{st} = \alpha v_{st} \frac{\Delta \rho}{\rho}, \quad (33)$$

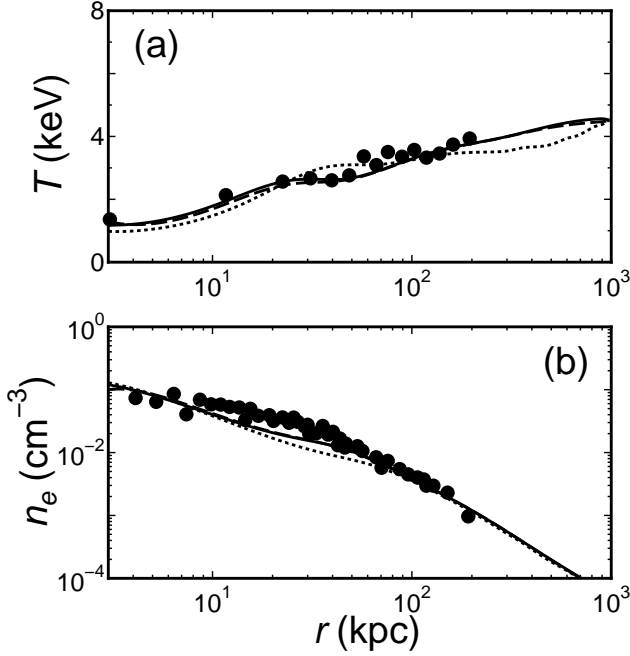


Figure 4. Same as Fig. 1 but for A2597. Filled circles represent observations (McNamara et al. 2001).

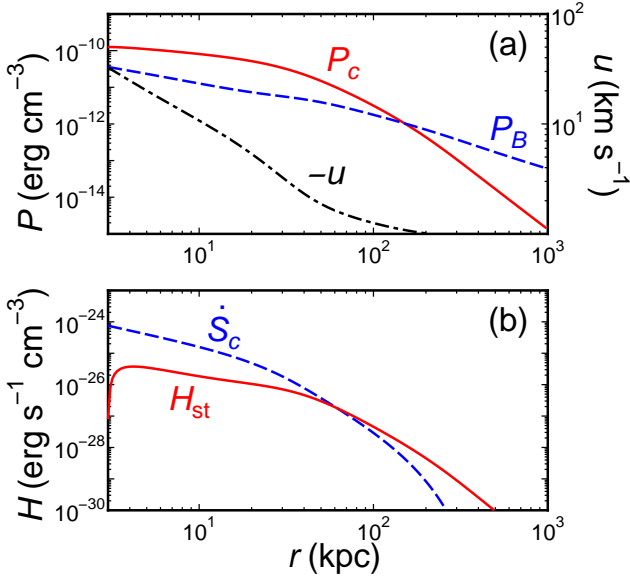


Figure 5. Profiles of (a) CR pressure (solid), magnetic pressure (dashed), and gas velocity (dot-dashed), (b) heating rate of CR streaming (solid) and CR injection rate (dashed) for A1795.

$$\begin{aligned} \Delta(\nabla \cdot \mathbf{v}_{\text{st}}) &= -v_{\text{st}} \left(\frac{2\xi}{r^2} + \frac{\alpha}{\rho} \frac{\partial \xi}{\partial r} \frac{\partial \rho}{\partial r} \right) \\ &+ \alpha v_{\text{st}} \frac{\Delta \rho}{\rho} \left(\frac{2}{r} + \frac{\alpha}{\rho} \frac{\partial \rho}{\partial r} \right) + \alpha v_{\text{st}} \frac{\partial}{\partial r} \left(\frac{\Delta \rho}{\rho} \right), \end{aligned} \quad (34)$$

$$\begin{aligned} \Delta H_{\text{st}} &= -v_{\text{st}} \left(\alpha \frac{\Delta \rho}{\rho} - \frac{\partial \xi}{\partial r} \right) \frac{\partial P_c}{\partial r} \\ &- v_{\text{st}} \left[P_c \frac{\partial}{\partial r} \left(\frac{\Delta P_c}{P_c} \right) + \frac{\Delta P_c}{P_c} \frac{\partial P_c}{\partial r} \right], \end{aligned} \quad (35)$$

respectively. In the above equations, the density perturbation can be replaced by $\Delta \rho / \rho = -\nabla \cdot \boldsymbol{\xi}$ (eq. [28]).

Equations (6) and (7) show that the source of CRs can be rewritten as $\dot{S}_c = Q(r)\dot{M}$. We can write the perturbation of the source as

$$\Delta \dot{S}_c = \left(\frac{\Delta Q}{Q} + \frac{\Delta \dot{M}_{\text{in}}}{\dot{M}} \right) \dot{S}_c, \quad (36)$$

where $\Delta \dot{M}_{\text{in}}$ is the perturbation of the mass flow rate at $r = r_{\text{in}}$. The perturbations in equation (36) are

$$\Delta Q = \frac{dQ}{dr} \xi, \quad (37)$$

$$\Delta \dot{M}_{\text{in}} = \frac{\dot{M}}{u_{\text{in}}} \frac{\partial \xi}{\partial t} \Big|_{r_{\text{in}}}, \quad (38)$$

where $u_{\text{in}} = u(r_{\text{in}})$.

We take ξ , ΔT , and ΔP_c as independent variables. We seek linear eigenmodes that behave as $\sim e^{\sigma t}$ with time. Equations (30)–(32) may be rewritten as

$$\begin{aligned} \left(\frac{P_g}{\rho} - u^2 \right) \frac{d}{dr} (\nabla \cdot \boldsymbol{\xi}) &= \left(r\sigma^2 - r \frac{dg}{dr} \right) \frac{\xi}{r} + \frac{1}{\rho} \frac{d}{dr} \left(P_g \frac{\Delta T}{T} \right) \\ -2u^2 \frac{d}{dr} \left(\frac{\xi}{r} \right) &+ \left(2\sigma u + u \frac{du}{dr} - \frac{1}{\rho} \frac{dP_g}{dr} \right) \frac{d\xi}{dr}, \end{aligned} \quad (39)$$

$$\begin{aligned} \left(\frac{P_g \sigma}{\gamma_g - 1} + \rho T \mathcal{L}_T + \frac{u}{\gamma_g - 1} \frac{dP_g}{dr} - \frac{\gamma_g u}{\gamma_g - 1} \frac{P_g}{\rho} \frac{d\rho}{dr} \right) \frac{\Delta T}{T} \\ + (P_g \sigma - \rho^2 \mathcal{L}_\rho - H_{\text{st}}) (\nabla \cdot \boldsymbol{\xi}) - \Delta H_{\text{st}} \\ + P_g u \frac{d}{dr} (\nabla \cdot \boldsymbol{\xi}) + \frac{P_g u}{\gamma_g - 1} \frac{d}{dr} \left(\frac{\Delta T}{T} \right) = 0, \end{aligned} \quad (40)$$

$$\begin{aligned} \sigma \frac{\Delta P_c}{P_c} + (v_{\text{st}} + u) \frac{d}{dr} \left(\frac{\Delta P_c}{P_c} \right) + \sigma \gamma_c (\nabla \cdot \boldsymbol{\xi}) + \gamma_c u \frac{\partial}{\partial r} (\nabla \cdot \boldsymbol{\xi}) \\ + \gamma_c \Delta (\nabla \cdot \mathbf{v}_{\text{st}}) = \frac{\Delta \dot{S}_c}{P_c} - \frac{\dot{S}_c \Delta P_c}{P_c^2}. \end{aligned} \quad (41)$$

We omit the dependence of $e^{\sigma t}$ hereafter. Equations (39)–(41) are first-order differential equations for the four variables ξ/r , $\Delta T/T$, $\Delta P_c/P_c$, and $d(\xi/r)/dr$. We numerically solve these equations as an eigenvalue problem, where the eigenvalue is the growth rate σ (Kim & Narayan 2003; Guo, Oh, & Ruszkowski 2008), using *Mathematica 9*. Following the previous studies, we set five boundary conditions. At the inner boundary ($r = r_{\text{in}}$), we give three conditions:

$$\xi/r = 1, \quad (42)$$

$$\frac{d}{dr} \left(\frac{\xi}{r} \right) = 0, \quad (43)$$

$$\begin{aligned} \Delta(r^2 \tilde{u} P_c) &= 2(u + v_{\text{st}}) P_c r \xi \\ &+ \left(\sigma \xi + u \frac{\partial \xi}{\partial r} + \Delta v_{\text{st}} \right) P_c r^2 + r^2 (u + v_{\text{st}}) \Delta P_c \\ &= 0. \end{aligned} \quad (44)$$

Equation (42) is a normalisation condition, and equation (43) guarantees the regularity of the solutions. Equation (44) means that the perturbed CR flux is zero at the cluster centre. At the outer boundary ($r = r_{\text{out}}$), we adopt the two conditions:

$$\xi = 0, \quad (45)$$

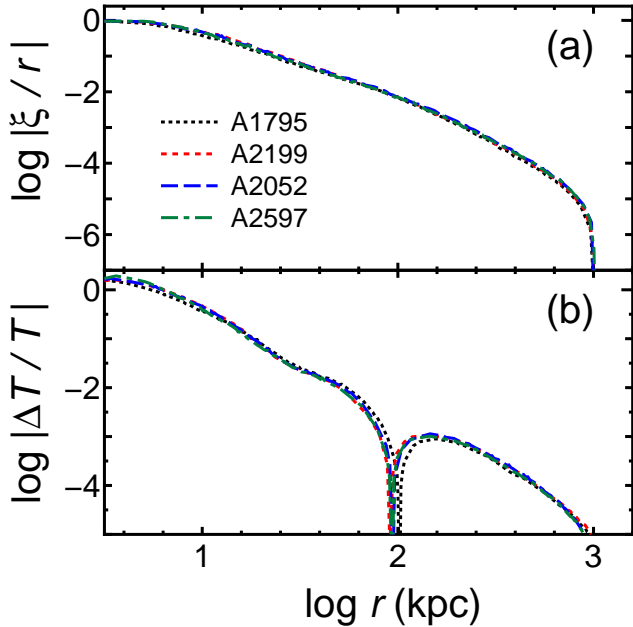


Figure 6. Eigenfunctions of the stable mode for A1795 (dotted), A2199 (short-dashed), A2057 (long-dashed), and A2597 (dot-dashed) plotted as functions of radius. (a) ξ/r , (b) $\Delta T/T$. The streaming velocity is $v_{\text{st}} = v_A$.

$$\Delta T = 0, \quad (46)$$

because the cooling time of the ICM is much larger than the cluster age.

The background ICM and CR profiles are given by the steady state solutions derived in § 3.1. We search σ that satisfies equations (39)–(41) and boundary conditions (42)–(46) in the range of $(10^4 \text{ Gyr})^{-1} < \sigma < (10^{-4} \text{ Gyr})^{-1}$. Since the equations are rather complicated, it takes a long time to find solutions. Thus, we limited our search to real σ and did not search imaginary σ . Following Kim & Narayan (2003) and Guo, Oh, & Ruszkowski (2008), we first fix σ and give arbitrarily $\Delta T/T$ at $r = r_{\text{in}}$. We then integrate equations (39)–(41) from $r = r_{\text{in}}$ to $r = r_{\text{out}}$ and check whether the first outer boundary condition (45) are satisfied. If not, we try another ΔT . We use the second outer boundary condition (46) as a discriminant for solutions.

As a result, we could not find any solutions with positive σ in the above range for the four clusters. This means that perturbations do not grow and the steady state solutions are quite stable even if we do not include thermal conduction, which has often been used to stabilise heating. On the other hand, we found decaying modes ($\sigma < 0$). Fig. 6 shows the eigenfunctions for the lowest order mode. For the mode shown in the figure, $-\sigma \sim 0.3 \text{ Gyr}^{-1}$ for the four clusters.

3.2.2 Numerical Simulations

In the analysis in § 3.2.1, we did not perform a complete parameter search; we did not examine imaginary σ and local instabilities, for example. Thus, in this subsection, we supplementarily study the stability of the steady state solutions using numerical simulations. We solve equations (1)–(4) with $\kappa = D = H_{\text{coll}} = \Gamma_{\text{loss}} = \partial P_B / \partial r = 0$. The hydrodynamic

part of the equations is solved by a second-order advection upstream splitting method (AUSM) based on Liou & Steffen (1993). We use 300 unequally spaced meshes in the radial coordinate to cover a region with a radius of $r_{\text{out}} = 1 \text{ Mpc}$. The inner boundary is set at $r_{\text{in}} = 3 \text{ kpc}$. The innermost mesh has a width of 90 pc, and the width of the outermost mesh is 17 kpc. While variables have zero gradients at the inner boundary, density and pressure are fixed at their initial values at the outer boundary. We use the steady state solutions obtained in § 3.1 as initial conditions ($t = 0$).

Figs. 1-4 show the results of the calculations. For all the four clusters, the ICM is stably heated at least within the age of the Universe ($t \sim 14 \text{ Gyr}$). For A2199, A2057, and A2597, profiles are almost identical to the initial ones at $t \lesssim 40 \text{ Gyr}$. However, local instabilities start developing at $t \gtrsim 40 \text{ Gyr}$ at $r \sim 50 \text{ kpc}$ and it later affects the inner profiles. In fact, it has been indicated that the heating via CR streaming is not locally stable (Loewenstein, Zweibel, & Begelman 1991; Pfrommer 2013). For A1795, the local instabilities do not develop until $t = 100 \text{ Gyr}$.

Although the local instabilities develop for the three clusters, they are not very radical. We found that our assumption of smaller b contributes to the suppression of rapid development of the local instabilities. Since we assumed that $b = 0.4$, the Alfvén velocity is $v_A = B / \sqrt{4\pi\rho} \propto \rho^{-0.1}$. If excessive cooling increases ρ at the cluster centre for example, it reduces v_A there. The smaller v_A prevents CRs from escaping from the cluster centre and increases P_c and $|\partial P_c / \partial r|$ around the centre. Since $H_{\text{st}} \propto |\partial P_c / \partial r|$, the cluster centre is well-heated. The same mechanism should work when $v_{\text{st}} = c_s$, because excessive cooling reduces the streaming velocity. Using numerical simulations, we found that the local instabilities we discussed here are suppressed by moderate thermal conduction of the level of $\sim 1\%$ of the Spitzer conductivity.

4 DISCUSSION

4.1 Evolution with time

Because of possible cluster mergers and the change of AGN activities, it is likely that the ICM profiles sometimes deviate from the steady state solutions we studied above. Thus, we study the time scale in which the perturbed ICM profiles return to the steady ones.

As an example, we choose the ICM profile of the steady state solution for A1795 when $v_{\text{st}} = v_A$ as a fiducial profile (Table 1 and Fig. 1). In this model, the efficiency ϵ in equation (7) was $\epsilon = 2.5 \times 10^{-4}$. We change the efficiency and construct new steady state solutions, while fixing the boundary parameters (n_0 , T_{in} , T_{out} , and P_{c0}). We obtain $\dot{M} = 19.0 M_{\odot} \text{ yr}^{-1}$ and $39.4 M_{\odot} \text{ yr}^{-1}$ for $\epsilon = 5 \times 10^{-4}$ and 1×10^{-4} , respectively. Their temperature and density profiles are not much different from those in Fig. 1, because the boundary conditions are the same. Using those profiles as the initial ones, we numerically solve equations (1)–(4) with $\kappa = D = H_{\text{coll}} = \Gamma_{\text{loss}} = \partial P_B / \partial r = 0$ for $v_{\text{st}} = v_A$ and $\epsilon = 2.5 \times 10^{-4}$. This may be the situation where the heating efficiency of the central AGN suddenly changes at $t = 0$.

In Fig. 7, we show the evolution of \dot{M} , which is proportional to L_{AGN} . The mass flow rates oscillate on a time

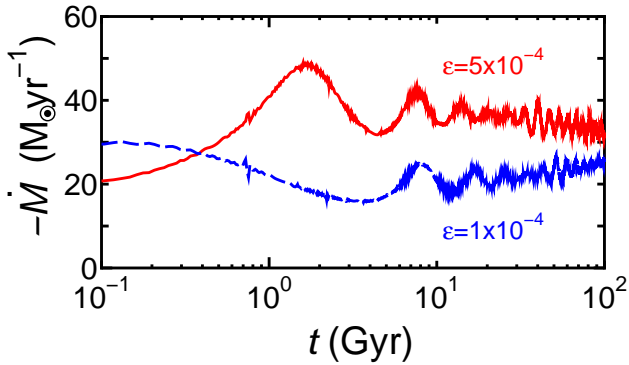


Figure 7. Evolution of \dot{M} for $\epsilon = 5 \times 10^{-4}$ (solid) and 1×10^{-4} (dashed) at $t = 0$.

scale of ~ 3 Gyr, which is comparable to the time scale of the decaying mode ($-1/\sigma$) that we studied in § 3.2.1. The amplitude of the oscillation gradually decreases and \dot{M} converges to that of the fiducial model of $\epsilon = 2.5 \times 10^{-4}$ ($\dot{M} = -27.1 M_{\odot} \text{ yr}^{-1}$). Since the time scale of the first large oscillation (~ 3 Gyr) is smaller than the cluster lifetime (~ 10 Gyr), we think that the discussions based on the steady state solutions are justified.

4.2 Radio mini-halos

In cool cores in some clusters, diffuse radio emissions called mini-halos have been observed. Our model predicts that the diffuse emissions originate from the CR protons heating the cluster cores (Paper III). In particular, the observed radio profiles can be nicely reproduced by our model. Recently, it has also been proposed that the CR electrons responsible for the radio emission have been accelerated by turbulence generated by the sloshing of the cool core gas (e.g. Mazzotta & Giacintucci 2008; ZuHone et al. 2013). Contrary to these models, our model does not require the sloshing because the CR protons are accelerated by the central AGNs.

While there is no direct relationship between the mini-halos and the sloshing in our model, an apparent relationship could be observed. In our model, mini-halos are associated with the AGNs that are active in cool cores. Meanwhile, structures related to the sloshing (e.g. cold fronts) are often produced around the cool cores (Fujita, Matsumoto, & Wada 2004; Ascasibar & Markevitch 2006). Moreover, in our model, the CR electrons responsible for the radio emission are created through the interaction between the CR protons and the target gas protons. Thus, more electrons are created in denser gas, and brighter radio emission would be observed in denser cores or on the denser side of a cold front associated with the sloshing. Of course, our model predicts that even clusters without sloshing can have the mini-halos. In the sloshing model, the morphology of the simulated mini-halos is complicated and depends on observing frequencies, because the sloshing is temporary and the CR acceleration occurs in the region where turbulence is developing (ZuHone et al. 2013). Thus, the radio emission could be strong even not at the cluster centre. This is not generally true in our model. be-

cause the radio emission tends to be strong at the cluster centre where the gas and CR densities are the highest.

On the other hand, we do not think that our model can explain Mpc-scale radio halos that are often observed in merging clusters without cool cores, because AGNs are active in cool cores, and dense gas in cool cores is required to produce the CR electrons. Those Mpc-scale radio halos may be produced by electrons accelerated in turbulence in the ICM (Brunetti et al. 2001; Petrosian 2001; Ohno, Takizawa, & Shibata 2002; Fujita, Takizawa, & Sarazin 2003; Brunetti & Lazarian 2011).

5 CONCLUSIONS

We have investigated the stability of CR heating in clusters. The CRs are accelerated at the central AGNs, and heat the ICM through CR streaming. First, we obtained steady state solutions of the ICM and CR profiles so that they are consistent with observations. The solutions are obtained when the magnetic fields are strong enough and their association with the ICM is relatively weak. Then, we analysed the stability of the solutions analytically and numerically. For the analytic approach, we adopted a Lagrangian stability analysis and found that there are no globally unstable modes. For the numerical approach, we followed the evolution of the solutions for 100 Gyr and confirmed that the solutions are quite stable. These results, as well as the consistency with radio observations (Paper III), make the CR heating an attractive solution of the cooling flow problem.

ACKNOWLEDGMENTS

We appreciate the referee’s useful comments. We thank F. Takahara, T. Tsuribe, D. Nagai, and L. Rudnick for useful discussion. This work was supported by KAKENHI (Y. F.: 23540308, Y. O.: 24.8344).

REFERENCES

- Ascasibar Y., Markevitch M., 2006, *ApJ*, 650, 102
- Blanton E. L., Randall S. W., Clarke T. E., Sarazin C. L., McNamara B. R., Douglass E. M., McDonald M., 2011, *ApJ*, 737, 99
- Boehringer H., Morfill G. E., 1988, *ApJ*, 330, 609
- Bregman J. N., Fabian A. C., Miller E. D., Irwin J. A., 2006, *ApJ*, 642, 746
- Brunetti G., Lazarian A., 2011, *MNRAS*, 412, 817
- Brunetti G., Setti G., Feretti L., Giovannini G., 2001, *MNRAS*, 320, 365
- Chen Y., Reiprich T. H., Böhringer H., Ikebe Y., Zhang Y.-Y., 2007, *A&A*, 466, 805
- Colafrancesco S., Dar A., De Rújula A., 2004, *A&A*, 413, 441
- Duffy A. R., Schaye J., Kay S. T., Dalla Vecchia C., 2008, *MNRAS*, 390, L64
- Enßlin T., Pfrommer C., Miniati F., Subramanian K., 2011, *A&A*, 527, A99
- Ettori S., Fabian A. C., Allen S. W., Johnstone R. M., 2002, *MNRAS*, 331, 635

Ettori S., Gastaldello F., Leccardi A., Molendi S., Rossetti M., Buote D., Meneghetti M., 2010, *A&A*, 524, A68
 Fabian A. C., 1994, *ARA&A*, 32, 277
 Felice G. M., Kulsrud R. M., 2001, *ApJ*, 553, 198
 Fujita Y., Matsumoto T., Wada K., 2004, *ApJ*, 612, L9
 Fujita Y., Ohira Y., 2011, *ApJ*, 738, 182 (Paper I)
 Fujita Y., Ohira Y., 2012, *ApJ*, 746, 53 (Paper II)
 Fujita Y., Ohira Y., 2013, *MNRAS*, 428, 599 (Paper III)
 Fujita Y., Suzuki T. K., 2005, *ApJ*, 630, L1
 Fujita Y., Takahara F., 1999, *ApJ*, 519, L55
 Fujita Y., Takizawa M., Sarazin C. L., 2003, *ApJ*, 584, 190
 Fukushima T., Makino J., 1997, *ApJ*, 477, L9
 Guo F., Oh S. P., 2008, *MNRAS*, 384, 251
 Guo F., Oh S. P., Ruszkowski M., 2008, *ApJ*, 688, 859
 Holman G. D., Ionson J. A., Scott J. S., 1979, *ApJ*, 228, 576
 Horner D. J., Mushotzky R. F., Scharf C. A., 1999, *ApJ*, 520, 78
 Ikebe Y., et al., 1997, *ApJ*, 481, 660
 Johnstone R. M., Allen S. W., Fabian A. C., Sanders J. S., 2002, *MNRAS*, 336, 299
 Jubelgas M., Springel V., Enßlin T., Pfrommer C., 2008, *A&A*, 481, 33
 Kaastra J. S., Ferrigno C., Tamura T., Paerels F. B. S., Peterson J. R., Mittaz J. P. D., 2001, *A&A*, 365, L99
 Kim W.-T., Narayan R., 2003, *ApJ*, 596, 889
 Liou, M.-S., & Steffen, C. J. 1993, *Journal of Computational Physics*, 107, 23
 Loewenstein M., Zweibel E. G., Begelman M. C., 1991, *ApJ*, 377, 392
 Longair, M. S., 1994, *High Energy Astrophysics*, second edition, Cambridge Univ. Press, Cambridge, vol. 2, § 20.4
 Makishima K., et al., 2001, *PASJ*, 53, 401
 Mathews W. G., Faltenbacher A., Brighenti F., 2006, *ApJ*, 638, 659
 Matsushita K., Belsole E., Finoguenov A., Böhringer H., 2002, *A&A*, 386, 77
 Mazzotta P., Giacintucci S., 2008, *ApJ*, 675, L9
 McNamara B. R., Nulsen P. E. J., 2012, *New Journal of Physics*, 14, 055023
 McNamara B. R., et al., 2001, *ApJ*, 562, L149
 Navarro J. F., Frenk C. S., White S. D. M., 1997, *ApJ*, 490, 493
 Ohno H., Takizawa M., Shibata S., 2002, *ApJ*, 577, 658
 Okabe N., Takada M., Umetsu K., Futamase T., Smith G. P., 2010, *PASJ*, 62, 811
 Peterson J. R., et al., 2001, *A&A*, 365, L104
 Petrosian V., 2001, *ApJ*, 557, 560
 Pfrommer C., 2013, arXiv, arXiv:1303.5443
 Pfrommer C., Enßlin T. A., Springel V., Jubelgas M., Dolag K., 2007, *MNRAS*, 378, 385
 Rephaeli Y., 1979, *ApJ*, 227, 364
 Rephaeli Y., 1987, *MNRAS*, 225, 851
 Rephaeli Y., Silk J., 1995, *ApJ*, 442, 91
 Rybicki G. B., & Lightman, A. P. 1979, *Radiative Processes in Astrophysics* (New York: Wiley)
 Sarazin C. L., 1986, *Reviews of Modern Physics*, 58, 1
 Schlickeiser R., 2002, *Cosmic Ray Astrophysics*, p. 291 (Berlin: Springer)
 Shapiro S. L., & Teukolsky, S. A. 1983, *Black Holes, White Dwarfs, and Neutron Stars* (New York: Wiley)

Sikora M., Begelman M. C., Madejski G. M., Lasota J.-P., 2005, *ApJ*, 625, 72
 Tamura T., et al., 2001, *A&A*, 365, L87
 Toma K., Takahara F., 2012, *ApJ*, 754, 148
 Tucker W. H., Rosner R., 1983, *ApJ*, 267, 547
 Wiener J., Oh S., Guo F., 2013, arXiv, arXiv:1303.4746
 ZuHone J. A., Markevitch M., Brunetti G., Giacintucci S., 2013, *ApJ*, 762, 78

APPENDIX A: SOUND VELOCITY CASE

Here, we consider the case where the streaming velocity is the sound velocity of the ICM ($v_{\text{st}} = c_s$). We set $P_B = 0$ because v_{st} does not depend on magnetic fields.

A1 Steady State Solutions

The steady state solutions can be obtained by replacing v_A by c_s in § 3.1. We solve equations (15)–(17) with boundary conditions (18)–(21). In order to match the solutions with observations, we adjust n_0 , T_{in} , and P_{c0} , while T_{out} is unchanged from that in § 3.1. We found that $P_{c0}/P_{g0} \sim 0.01$ – 0.1 from comparison with radio observations (Fig. 14 in Paper III). Thus, we assume that $P_{c0}/P_{g0} = 0.03$ for all the four clusters.

The dashed lines in Figs. A1–A4 show the steady state solutions for the four clusters. The temperature and density profiles generally reproduce the observations. The parameters we adopted are shown in Table 1 ($v_{\text{st}} = c_s$). Fig. A5 shows the profiles of P_c , u , H_{st} , and \dot{S}_c for the steady state solution of A1795. The results are qualitatively the same for the other clusters. Compared to Fig. 5a, P_c is smaller because $v_{\text{st}} = c_s$ is larger than v_A , and it enhances the escape of the CRs (Fig. A5a). Fig. A5b shows that the heating (H_{st}) is more widely distributed than the CR injection (\dot{S}_c) as is the case of $v_{\text{st}} = v_A$ (Fig. 5b).

A2 Stability Analysis

A2.1 Lagrangian Perturbation Analysis

As we did in § 3.2.1, we solve equations (39)–(41) under the five boundary conditions (42)–(46). However, the terms including v_{st} (equations. [33]–[35]) must be modified.

Since we assumed that $v_{\text{st}} = c_s \propto T^{1/2}$, perturbations of v_{st} can be represented by

$$\Delta v_{\text{st}} = \frac{v_{\text{st}}}{2} \frac{\Delta T}{T}, \quad (\text{A1})$$

$$\begin{aligned} \Delta(\nabla \cdot \mathbf{v}_{\text{st}}) = & -v_{\text{st}} \left(\frac{2\xi}{r^2} + \frac{1}{2T} \frac{\partial \xi}{\partial r} \frac{\partial T}{\partial r} \right) \\ & + v_{\text{st}} \frac{\Delta T}{T} \left(\frac{1}{r} + \frac{1}{4T} \frac{\partial T}{\partial r} \right) + \frac{v_{\text{st}}}{2} \frac{\partial}{\partial r} \left(\frac{\Delta T}{T} \right). \end{aligned} \quad (\text{A2})$$

The perturbation of the heating by the CR streaming is

$$\begin{aligned} \Delta H_{\text{st}} = & -v_{\text{st}} \left(\frac{1}{2} \frac{\Delta T}{T} - \frac{\partial \xi}{\partial r} \right) \frac{\partial P_c}{\partial r} \\ & - v_{\text{st}} \left[P_c \frac{\partial}{\partial r} \left(\frac{\Delta P_c}{P_c} \right) + \frac{\Delta P_c}{P_c} \frac{\partial P_c}{\partial r} \right]. \end{aligned} \quad (\text{A3})$$

The background ICM and CR profiles are given by the

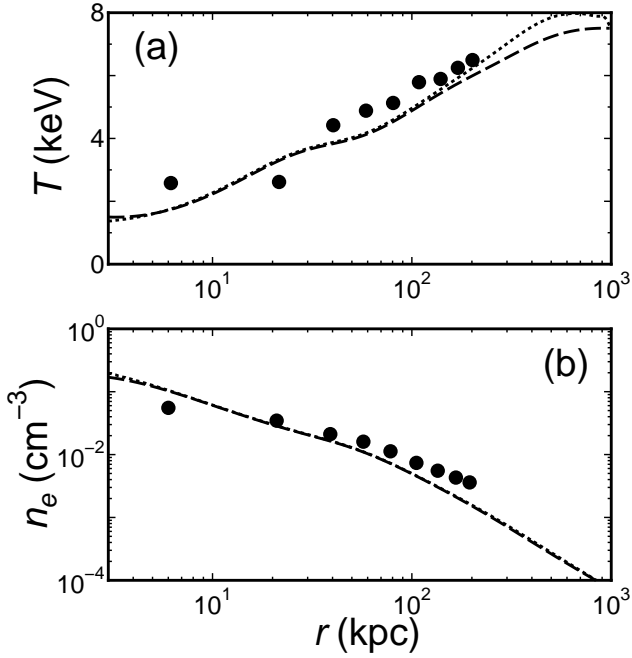


Figure A1. (a) Temperature and (b) density profiles for A1795. Dashed lines show the steady state solution or the initial profiles for the numerical simulation. Dotted lines are the results of numerical simulation at 100 Gyr. Filled circles represent observations (Ettori et al. 2002). Error bars are omitted.

steady state solutions derived in § A1. We search σ that satisfies equations (39)–(41) and boundary conditions (42)–(46) in the range of $(10^4 \text{ Gyr})^{-1} < \sigma < (10^{-4} \text{ Gyr})^{-1}$. As is the case of $v_{\text{st}} = v_A$, we could not find any solutions with positive σ in the above range for the four clusters. On the other hand, we found decaying modes ($\sigma < 0$). Fig. A6 shows the eigenfunctions for the lowest order mode. For the mode shown in the figure, $-\sigma = 0.4, 0.4, 0.2,$ and 0.3 Gyr^{-1} for A1795, A2199, A2057, and A2597, respectively.

A2.2 Numerical Simulations

As we did in § 3.2.2, we numerically solve equations (1)–(4) with $\kappa = D = H_{\text{coll}} = \Gamma_{\text{loss}} = \partial P_B / \partial r = 0$ for $v_{\text{st}} = c_s$. The initial ($t = 0$) profiles are given by the steady state solutions we obtained in § A1.

Dotted lines in Figs. A1–A4 show the profiles at $t = 100 \text{ Gyr}$. They are almost identical to those at $t = 0$ (dashed lines). Contrary to the case of $v_{\text{st}} = v_A$ (§ 3.2.2), local instabilities do not develop for $t < 100 \text{ Gyr}$ for all the four clusters. The results indicate that the steady solutions are very stable.

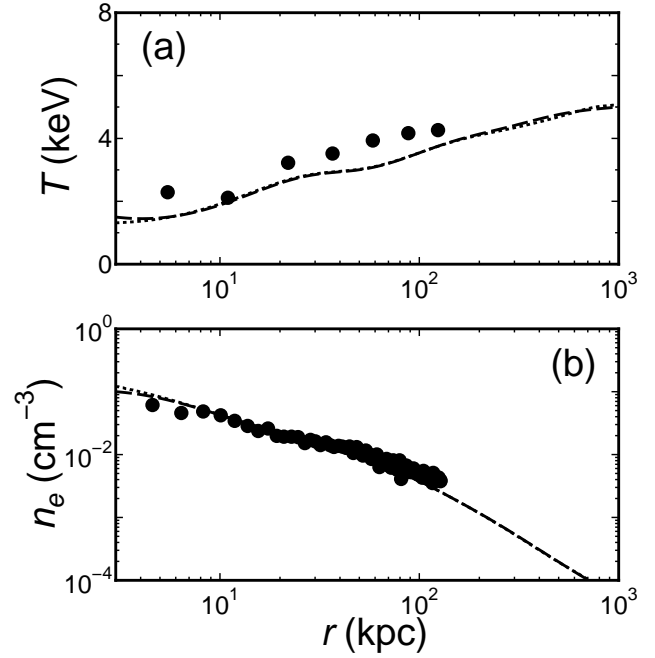


Figure A2. Same as Fig. A1 but for A2199. Filled circles represent observations (Johnstone et al. 2002).

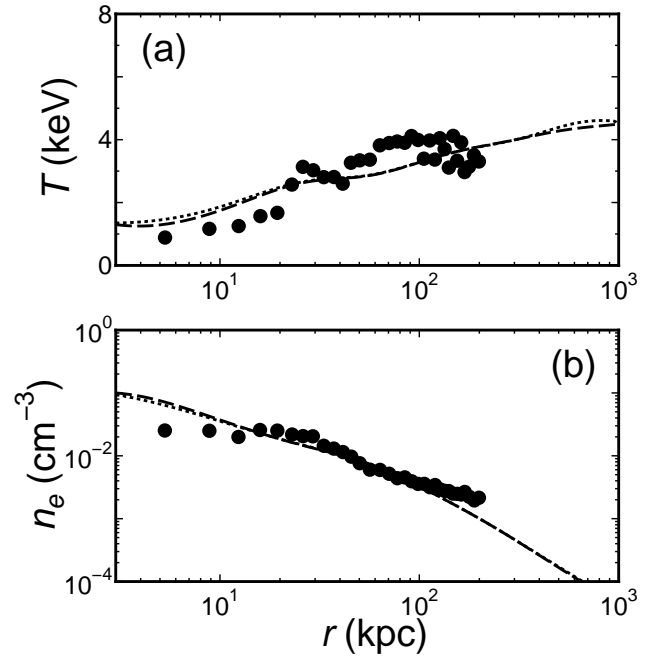


Figure A3. Same as Fig. A1 but for A2052. Filled circles represent observations (Blanton et al. 2011).

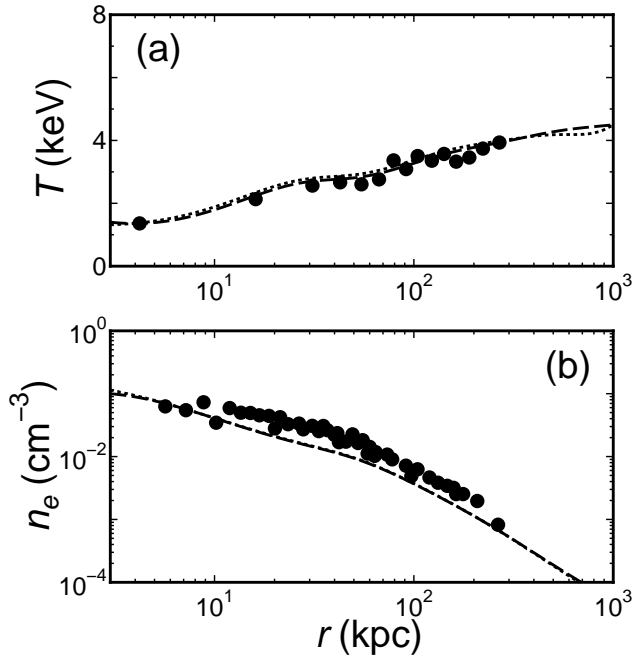


Figure A4. Same as Fig. A1 but for A2597. Filled circles represent observations (McNamara et al. 2001).

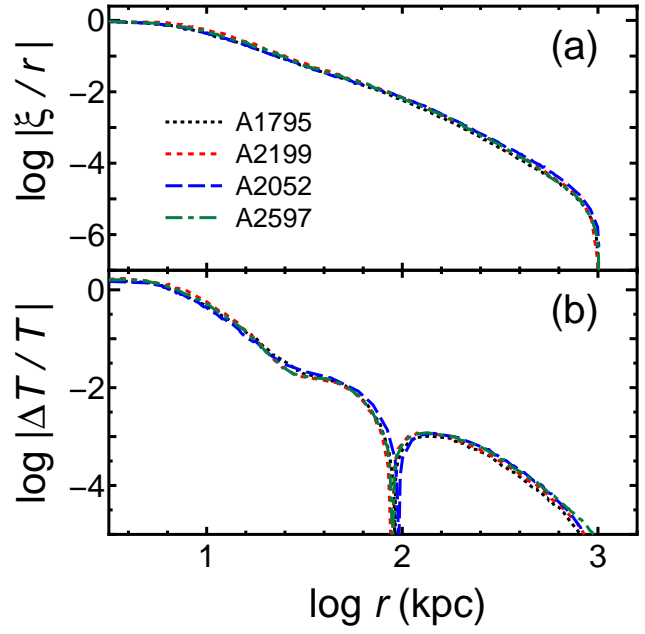


Figure A6. Same as Fig. 6 but for $v_{st} = c_s$

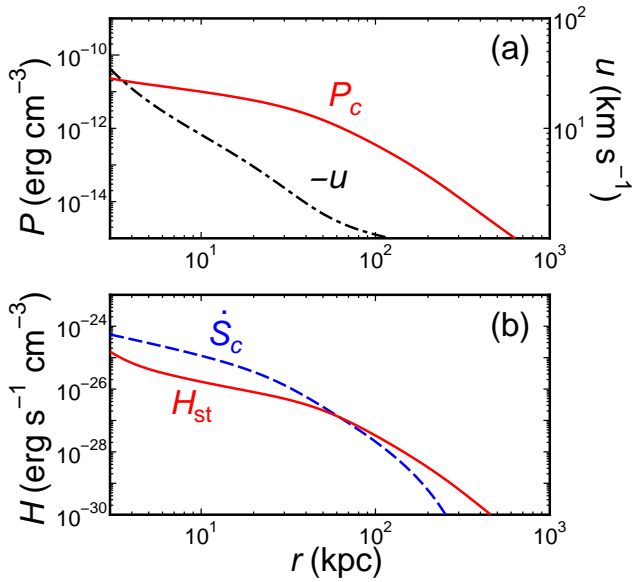


Figure A5. Profiles of (a) CR pressure (solid) and gas velocity (dot-dashed), (b) heating rate of CR streaming (solid) and CR injection rate (dashed) for A1795.